Optically determined minority-carrier transport in GaAs/$Al_xGa_{1-x}As$ heterostructures

D. J. Wolford, G. D. Gilliland, T. F. Kuech,* and J. A. Bradley
IBM Research Division, Thomas J. Watson Research Center, P.O. Box 218, Yorktown Heights, New York 10598

H. P. Hjalmarson
Sandia National Laboratories, Albuquerque, New Mexico 87185
(Received 8 April 1992)

We have studied minority-carrier electron and hole transport versus temperature (30–300 K) in a series of undoped, "interface-free," GaAs/$Al_{0.3}Ga_{0.7}As$ double heterostructures prepared by organometallic vapor-phase epitaxy, with GaAs thicknesses from 0.1 to 10 μm. This was achieved using an all-optical, time-resolved photoluminescence-imaging technique with a spatial resolution of $\lesssim 3$ μm, temporal resolution of ~ 50 ps, and spectral resolution of < 1 cm^{-1}. This technique allows direct determination of minority-carrier transport properties, and is superior to electrical transport measurement techniques in that it is contactless, may distinguish between diffusive and nondiffusive carrier motion, and has high temporal and spectral resolution. We find all transport (electron and hole) in these structures to be diffusive. Specifically, transport in thick structures ($\gtrsim 0.5$ μm) is hole-dominated ambipolar diffusion, whereas in thinner structures ($\lesssim 0.5$ μm) we observe a *time-dependent* transition from ambipolar to electron-dominated diffusion. Minority-carrier mobilities derived from these diffusion measurements, from 300 to ~ 30 K, are in excellent agreement with both electron and hole majority-carrier mobilities. Furthermore, fits to the temperature-dependent mobilities yield deformation potentials in agreement with published electrically derived values.

I. INTRODUCTION

Carrier transport in semiconductors is most commonly studied through Hall measurements.[1–8] This technique has been used ubiquitously to study majority-electron and -hole transport in high-purity, bulk GaAs,[3] undoped GaAs/$Al_xGa_{1-x}As$ quantum wells (QW's),[9,10] modulation-doped GaAs/$Al_xGa_{1-x}As$ QW structures,[11] and two-dimensional (2D) electron and hole gas (2DEG and 2DHG, respectively) transport in modulation-doped single GaAs/$Al_xGa_{1-x}As$ heterojunction structures.[12–19] Despite the obvious accomplishment of the Hall technique, there are other measurement techniques equally capable of quantifying carrier transport. Recently, an all-optical photoluminescence (PL) imaging technique, analogous to the classical Haynes-Shockley experiment,[20] has been used to measure, directly, carrier transport;[21–24] however, here, in contrast to electrical measurement techniques, the observed transport is dominated by *minority carriers* (rather than majority carriers). Many varieties of this PL-imaging technique, each with distinct advantages and disadvantages, have been used to measure transport, including time-of-flight measurements,[23] masked-PL imaging,[22] and direct-PL imaging.[21,24]

In this paper we use an all-optical, time-resolved PL-imaging technique to study electron and hole transport in ideal, "interface-free" GaAs structures. We measure, directly, the transport of minority carriers and examine, side by side, our optically determined diffusivities, as equivalent mobilities, with electrically determined mobilities in comparable structures. Our results, from ~ 30 K to room temperature, are in excellent agreement with classically derived majority-carrier mobilities. Thus, we find *minority-carrier* and *majority-carrier* transport, i.e., holes in *n*-type GaAs and holes in *p*-type GaAs, *quantitatively identical*, contrary to some predictions.[25]

II. EXPERIMENT

Our samples were simple GaAs/$Al_{0.3}Ga_{0.7}As$ double heterostructures. Such structures were chosen for several reasons. First, the wider band-gap $Al_{0.3}Ga_{0.7}As$ layers effectively confine photoexcited carriers to the GaAs layer, thereby eliminating major nonradiative decay processes which may occur at the substrate and free surface. In addition, we find nonradiative decay at GaAs/$Al_{0.3}Ga_{0.7}As$ heterointerfaces to be *virtually nonexistent* in these ideal structures,[26] yielding minority-carrier lifetimes which are extremely long (> 2.5 μs) and PL efficiencies which are very high (10^3–10^4 greater than for bare GaAs epilayers). Second, $Al_{0.3}Ga_{0.7}As$ layers are transparent to near-resonant excitation of the GaAs layer. Therefore, photoexcited carriers are generated solely in the GaAs layer, and our measured results characterize the transport in the active-GaAs layer only—thereby eliminating the common difficulty in Hall measurements of determining the location of the conducting layer or channel. Lastly, such simple structures ease the interpretation of results. The samples were grown by organometallic vapor-phase epitaxy (OMVPE) at 750 °C, at a calibrated growth rate of $\simeq 350$ Å/min. All layers were nominally undoped; $Al_{0.3}Ga_{0.7}As$ layers were *p* type ($\sim 3\times10^{16}$ cm^{-3}) and 0.5 μm thick, while GaAs layers were *n* type ($\sim 1\times10^{15}$ cm^{-3}) with thicknesses ranging from 0.1 to 10.0 μm.

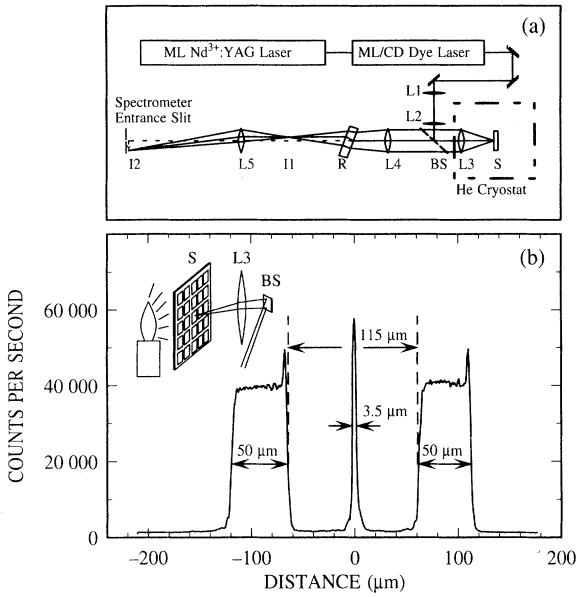

FIG. 1. (a) Experimental setup for spatially resolved PL measurements ($L1$–$L5$, lenses; BS, beamsplitter; S, sample; $I1$,$I2$, PL images; and R, refractory block). (b) Spatial calibration of our system, obtained using a quartz disk in place of the sample, onto which aluminum squares (115×115 μm^2, and 50-μm spacing) were evaporated (inset); this was then backlighted and imaged, while simultaneously focusing the laser to a 3.5-μm spot size on one of the aluminum squares.

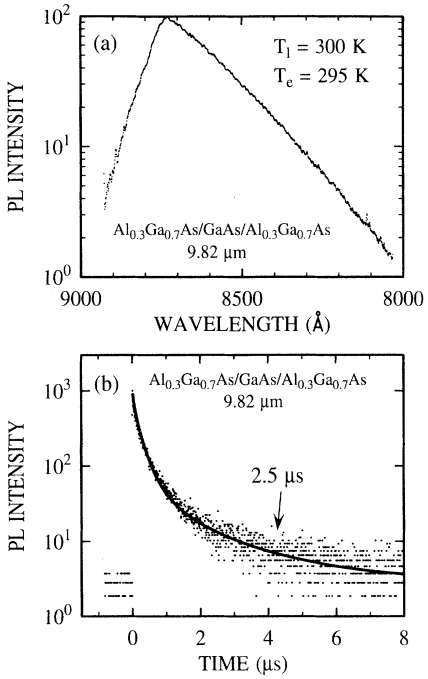

FIG. 2. (a) Room-temperature PL spectrum for the 9.82-μm GaAs-layer thickness double heterostructure. Solid line represents a Maxwell-Boltzmann fit, yielding the electronic temperature T_e. (b) Room-temperature PL time decay for the 9.82-μm double heterostructure. Solid line represents least-squares fit to the data with a bimolecular rate equation, yielding the 2.5-μs lifetime characteristic of the exponential tail.

Our all-optical technique for time-resolved PL imaging of minority-carrier transport requires excitation and imaging, in a confocal manner, through a specially designed microscope. Figure 1(a) illustrates the experimental apparatus. A mode-locked, synchronously pumped cavity-dumped dye laser (tunable from 6400–8400 Å) with a pulse width of $\sim$1 ps was used as a source of photoexcitation, with peak excitation densities possibly reaching $\sim5\times10^{18}$ cm^{-3}. Lenses $L3$, $L4$, and $L5$ form our "PL-imaging microscope," whereas lenses $L1$, $L2$, and $L3$ form our "laser focusing microscope." The system was designed with near-diffraction-limit focusing of the laser beam, magnification (of the PL image) of $\sim20\times$, and light-collecting f-number matched for the composite optical-imaging system, including the spectrometer. Scanning of the PL image across the spectrometer entrance slit was performed through rotation of a Plexiglas block, R, and its corresponding refraction of the back-scattered luminescence. Linearity in the imaging plane was confirmed over a sample spatial range of ±400 μm; Fig. 1(b) shows such spatial calibration of this system. For this calibration, a quartz disk, onto which aluminum squares were photolithographically defined and evaporated, was placed in the sample position. This calibration disk was then back lit with white light, while simultaneously focusing the laser beam onto one of the aluminum squares—thus yielding a "negative" image of the squares with a "δ-function" spike in the center (distance$=0$ μm) corresponding to the focused laser-beam spot. The resulting overall spatial resolution was ~3 μm—thus near diffraction limit.

III. ROOM-TEMPERATURE RESULTS

A typical room-temperature PL spectrum, together with the corresponding time decay from the same 9.82-μm-thick double heterostructure sample, is shown in Fig. 2. We find relatively intense PL resulting from free-carrier, band-to-band recombination. Fits to the high-energy side with the Maxwell-Boltzmann expression—indicative of thermalized band-to-band recombination—yield electronic temperatures virtually equal to the measured and known lattice temperature. Decay kinetics for these structures are somewhat more complicated and dependent upon the GaAs-layer thickness, but independent of PL-emission energy. We find that all decay kinetics, at all temperatures, are well understood and accurately modeled by rate equations for free-carrier recombination[27] (optical properties are dominated by *minority carriers*). Further, lifetimes obtained from fits to the data, representing the exponential tail of the decay, are extremely long ($\gtrsim2.5$ μs).[26,27] These fully understood decay kinetics, long lifetimes, and high PL efficiencies are crucial in making possible studies such as ours discussed below.

Figures 3(a) and 3(b) show time- and spatially-resolved PL distributions for our 9.82- and 0.30-μm-thick double heterostructures at 300 K. These data clearly show that the PL distribution, and, hence, minority-carrier spatial distribution, expands spatially with increasing time. If this minority-carrier transport should be diffusive, then

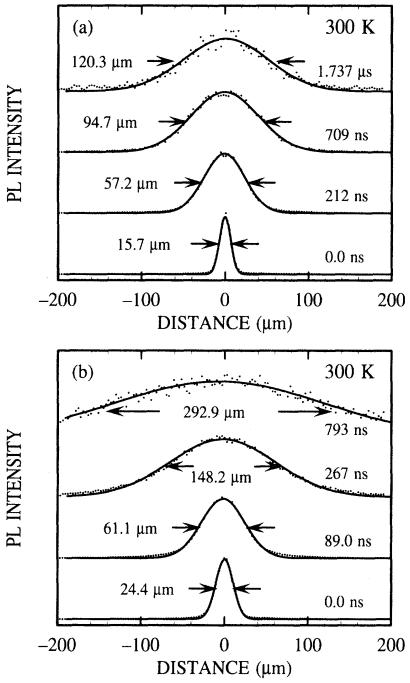

FIG. 3. Room-temperature time-resolved PL distributions. Solid lines represent Gaussian fits to data, with FWHM vs time shown. (a) Results for double heterostructure with 9.82-μm GaAs-layer thickness; (b) results for double heterostructure with 0.30-μm GaAs-layer thickness.

its spatial distribution should evolve in time according to the appropriate diffusion equation. Because our imaging technique only resolves the in-plane (parallel to the heterointerface) motion of carriers and our observed transport occurs over distances much larger than the GaAs-layer thickness, we use the cylindrically symmetric, two-dimensional diffusion equation,

$$\frac{\partial p(\mathbf{r},t)}{\partial t}=D\nabla^2 p(\mathbf{r},t)-\frac{p(\mathbf{r},t)}{\tau}\ , \tag{1}$$

to model the observed transport. The time-dependent minority-carrier spatial distributions may be obtained analytically from Eq. (1) as

$$p(\mathbf{r},t)=\frac{\Delta_0^2 p_0}{4Dt+\Delta_0^2}\exp\left[\frac{-r^2}{4Dt+\Delta_0^2}\right]\exp\left[-\frac{t}{\tau}\right]\ , \tag{2}$$

where Δ_0 is the initial ($t=0$) minority-carrier distribution, D is the diffusion constant, and τ is the minority-carrier lifetime. Here, we have assumed, for simplicity, that minority carriers decay exponentially. This is clearly not the case for all of our structures at all temperatures (e.g., bimolecular decays—see Fig. 2). However, we find, through numerical modeling, that with our experimental conditions these additional complexities yield virtually negligible modifications to the spatial distributions, in agreement with Olsson *et al.*[21] Further, such Gaussian distributions accurately model our data, indicated by the solid lines in Fig. 3. Most conspicuously, observed minority-carrier distributions expand macroscopically

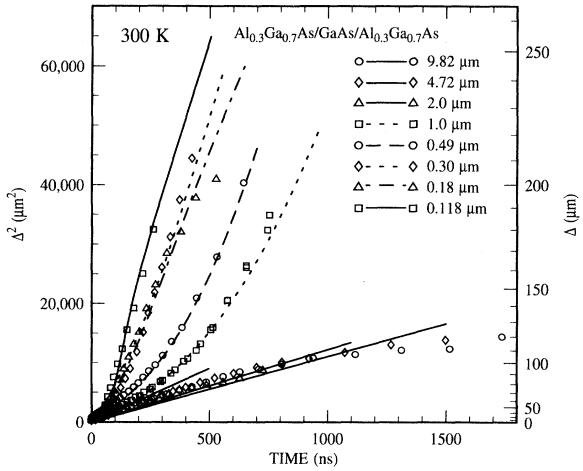

FIG. 4. Gaussian PL FWHM squared vs time $\Delta(t)^2$, for all $GaAs/Al_{0.3}Ga_{0.7}As$ double heterostructures at room temperature; lines represent fits to the data, as discussed in text.

from an initial full width at half maximum (FWHM), Δ_0, of ~ 4 μm to over *300 μm* during the minority-carrier lifetime.

We may further quantify these data by plotting the squared PL FWHM versus time, $\Delta^2(t)$, after the laser pulse, with results for all samples studied shown in Fig. 4. For diffusive transport, and corresponding Gaussian spatial distributions, Δ^2 should vary linearly with time as

$$\Delta^2(t)=[16\ln(2)]D_a t+4\ln(2)\Delta_0^2\ . \tag{3}$$

Figure 4 shows that our transport data are not linear versus time for all samples, but are for some, with clear, *systematic* trends for decreasing GaAs-layer thicknesses.

Results in Figs. 3 and 4 seem, initially, to be somewhat contradictory. The rigorously Gaussian PL distributions of Fig. 3 reflect the occurrence of diffusive transport for the relatively wide structures of GaAs thickness $\gtrsim 0.30$ μm, whereas more nonlinear behavior found in Fig. 4 for some narrower GaAs layers does not. All of these results may, nonetheless, be understood in the context of Eqs. (1)–(3), by taking into account the time-dependent (and carrier-density-dependent) ambipolar diffusion constant D_a. The ambipolar diffusion constant may be expressed as

$$D_a=\frac{[(n+n_0)+(p+p_0)]D_e D_h}{(n+n_0)D_e+(p+p_0)D_h}\ , \tag{4}$$

where D_e (D_h) is the electron (hole) diffusion constant, n (p) is the photoexcited electron (hole) density, and n_0 (p_0) is the built-in electron (hole) density. Equation (4) shows that D_a depends not only on the electron and hole diffusion constants, but the "relative" densities of electrons and holes. For nearly intrinsic or high-purity material ($n=p$ and $n_0\simeq p_0\simeq 0$), D_a is dominated by the smaller diffusion constant D_h. Additionally, Eq. (4) shows that D_a may be time dependent due to the time-dependent electron and hole densities and the nonzero built-in carrier densities. Such carrier-density- and time dependences may be accounted for by including (1) the

time-dependent photoexcited carrier densities obtained in our kinetic measurements, and (2) the static built-in carrier densities. In so doing, we find that the data in Fig. 4 may be accurately modeled in this way, with best fits shown as lines in the figure—thus reconciling the initial apparent discrepancies between Figs. 3 and 4, and confirming truly *diffusive* motion. We also find that the built-in hole density in the GaAs layer is not constant versus GaAs-layer thickness, but drastically increases inversely with GaAs thickness to $\sim 1\times 10^{18}$ cm^{-3} for sufficiently thin structures ($\lesssim 0.1$ μm), whereas $p_0 < n_0$ for thicker structures, consistent with our estimated compensation ($\simeq 40\%$).[28]

In totality, these results are consistent with the material parameters we have independently determined for these structures, and are interpretable as an *effective p-type modulation doping.* With the known doping level and thickness of each layer of our structures, the *p-n* junction depletion width in the GaAs layer is ~ 0.5 μm. Thus, holes from $Al_{0.3}Ga_{0.7}As$ layers may accumulate in the GaAs layer for GaAs layers thinner than approximately twice this depletion length (two interfaces). This is analogous to modulation doping, wherein majority carriers in the active layer originate from dopants (either intentional or residual) in another layer of the heterostructure. Accordingly, thick structures ($\gtrsim 0.5$ μm) are *inherently n type,* whereas thinner structures ($\lesssim 0.5$ μm) are *modulation-doped p type,* and the minority-carrier species changes from holes to electrons for sufficiently thin structures ($\lesssim 0.5$ μm). Thus, we observe a time-dependent transition from ambipolar- to electron-dominated transport.

From such analyses of our data, we calculate the electron and hole diffusion constants, shown in Fig. 5. Additionally, using the nondegenerate Einstein relation, $\mu = D|e|/kT$, both electron and hole mobilities may be obtained. (We will discuss later, in more detail, our justification in using the nondegenerate form of the Einstein relation below.) We find both electron and hole mobilities which are independent of GaAs-layer thickness, and *quantitatively* in agreement with electrical measurements on these same samples—$\mu = 5800$ cm^2/V s for electrons (majority carriers in the *n*-type GaAs layer)—and with reported values for both electron and hole mobilities obtained electrically at room temperature (horizontal lines in the figure).[3,29]

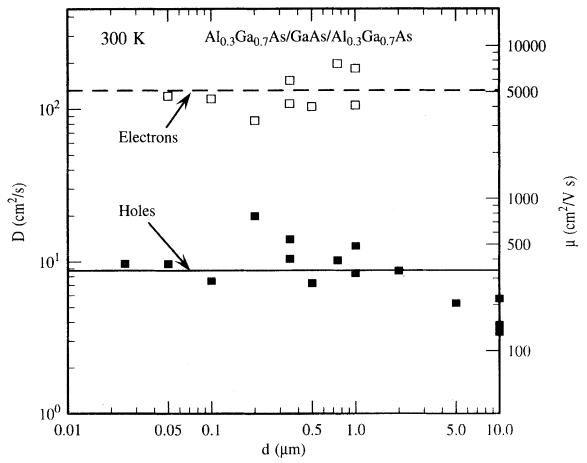

FIG. 5. Room-temperature electron and hole diffusion constants, and corresponding mobilities, vs GaAs-layer thickness obtained from analysis of data in Fig. 4. Horizontal lines represent typical electron and hole mobilities obtained electrically in high-purity *n*- and *p*-type GaAs.

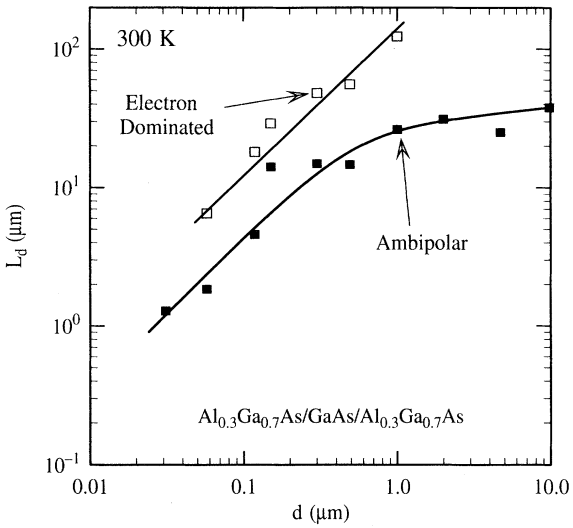

FIG. 6. Diffusion lengths vs GaAs-layer thickness at room temperature.

Minority-carrier diffusion lengths may be obtained as by-products of our decay kinetics and transport measurements. Defined as $L_d = \sqrt{D\tau}$, we find minority-electron diffusion lengths greater than *100 μm,* and minority-hole diffusion lengths of *~35 μm*—among the largest diffusion lengths reported for any GaAs structure.[30] These lengths shown in Fig. 6 also decrease with decreasing GaAs-layer thicknesses ($\lesssim 1.0$ μm), and this steady diminution may be attributed to the rapid decrease in minority-carrier lifetime we find for decreasing GaAs-layer thickness,[31] and is consistent with our asserted *p*-type modulation doping. Using this information, the heterointerfacial quality of our structures may also be characterized. We thus find that carriers move extreme distances during their lifetime, and, thus, may scatter from each heterointerface many times *without decaying nonradiatively.* Thus, our data indicate that carriers scatter from these high-quality heterointerfaces up to *~200 times* during their lifetime—signifying that these high-density heterointerfaces are "mirrorlike," reflecting carriers without suffering and/or competitive nonradiative decay.

IV. TEMPERATURE DEPENDENCE (300–30 K)

Figures 7 and 8 show, respectively, the temperature dependencies of the PL and PL decay kinetics for our 9.82-μm double heterostructure. As previously found at room temperature, the observed emission results from thermalized carriers and, thus, radiative band-to-band recombination. We find, again, these temperature-

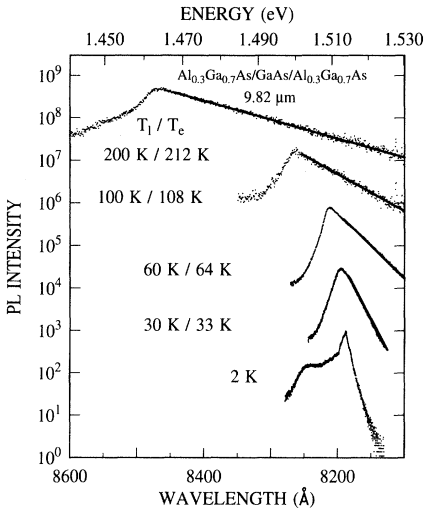

FIG. 7. PL spectra vs temperature for the 9.82-μm-thick double heterostructure. Electronic temperatures were obtained from Maxwell-Boltzmann fits to the spectra.

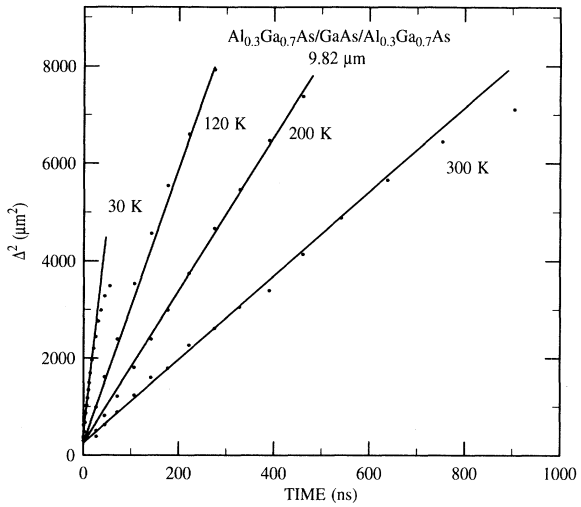

FIG. 9. Temperature dependence of Gaussian PL FWHM squared $\Delta^2(t)$ vs time for the 9.82-μm double heterostructure. Solid lines represent linear least-squares fits to data.

dependent kinetics, for all structures, are fully described by the appropriate temperature-dependent rate equations—taking into full account possible carrier freezeout.

The temperature dependence of the minority-carrier transport may be characterized and quantified in the same manner as our room-temperature results. We find Gaussian PL-spatial distributions at all temperatures (300–30 K). Figure 9 shows Δ^2 versus time obtained from such Gaussian fits to the data. These results, for our thickest heterostructure (9.82 μm), are *linear* at all temperatures, and thus represent the genuine diffusive transport of minority holes. Using Eq. (3), we find that the derived diffusion constant for this minority-hole transport increases with decreasing temperature. Similar measurements for our 0.30-μm structure versus temperature (300–30 K) yield results consistent with the *p*-type modulation doping found at room temperature, thus allowing a determination of *both* minority-electron and minority-hole transport, as shown in Fig. 10. Here also, we find diffusion constants [from fits to Eq. (4)], for both electrons and holes, which *increase* with decreasing temperature.

Figure 11 shows the temperature-dependent minority-hole mobility obtained from the 9.82-μm-thick heterostructure using the nondegenerate Einstein relation. Here, the carrier temperature is assumed equal to the lattice temperature—thus, justified from our findings that, at these temperatures, minority-carrier lifetimes are sufficiently long to allow complete carrier cooling to the lattice temperature, as has been evidenced in the PL

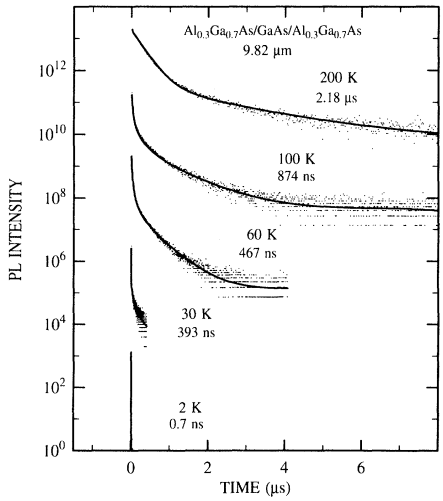

FIG. 8. PL decay kinetics vs temperature for the double heterostructure with a 9.82-μm GaAs-layer thickness. Lifetimes were obtained from fits, and correspond to the exponential tail of the decay.

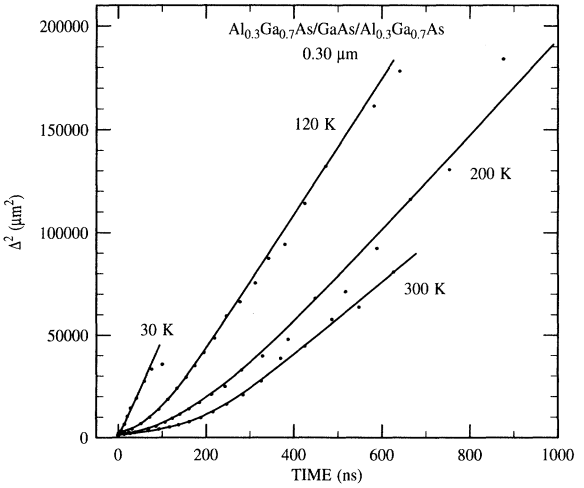

FIG. 10. Temperature dependence of Gaussian PL FWHM squared $\Delta^2(t)$ vs time for the 0.30-μm double heterostructure. Solid lines represent least-squares fits to data using Eq. (4).

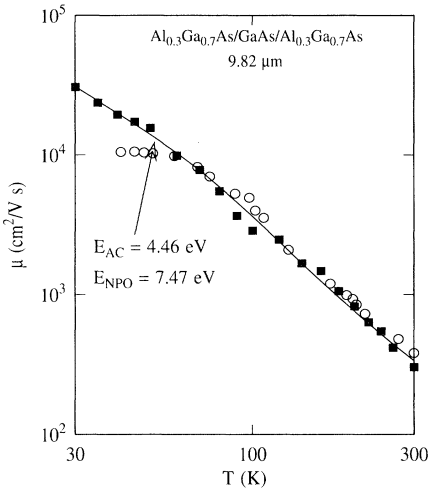

FIG. 11. Temperature dependence of minority-hole mobility in the 9.82-μm double heterostructure (■). Mobilities were obtained from the measured diffusion constants using the nondegenerate Einstein relation. Solid line represents best fit to data, yielding acoustic-phonon and nonpolar-optic-phonon deformation potentials. Hill's results (Ref. 34) for majority holes in p-type GaAs are also shown (○) with excellent agreement.

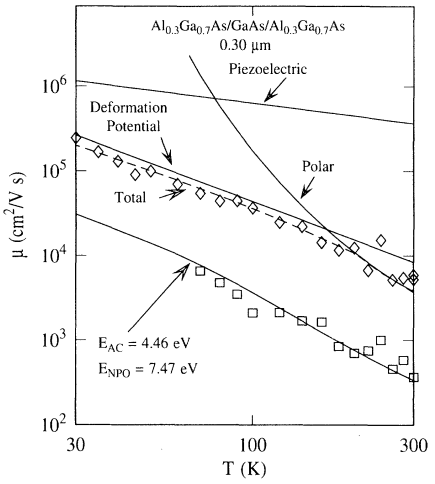

FIG. 12. Temperature dependence of minority-hole (□) and minority-electron (◇) mobilities in the 0.30-μm double heterostructure. Mobilities were obtained from the measured diffusion constants using the nondegenerate Einstein relation. Solid lines represent best fits to the data, as discussed in the text.

high-energy Maxwell-Boltzmann tails and their derived electronic temperatures, of Fig. 7. Further, utilization of the nondegenerate form of the Einstein relation is warranted by the relatively high lattice temperatures which preclude degeneracy and exciton formation.

Hole mobilities in GaAs, at these temperatures, are dominated by acoustic-phonon and nonpolar optical-phonon scattering. Using Wiley's formalism,[29,32,33] the combined mobility is

$$\mu_{\mathrm{AC,NPO}}=3.1727\times10^{-5}\frac{r^{5/2}(1+r^{1/2})}{(1+r^{3/2})^2}\times\frac{\rho\bar{u}^2}{(m_1^*/m_0)^{5/2}E_{\mathrm{AC}}^2}S(\theta,\eta,T)T^{-3/2}\ , \quad (5)$$

where

$$S(\theta,\eta,T)=\int_0^\infty\frac{xe^{-x}dx}{1+C[(1+\theta/xT)^{1/2}+e^{\theta/t}(1-\theta/xT)^{1/2}]}\ , \quad (6)$$

$$C=(\theta/T)\eta/2(e^{\theta/T}-1)\ , \quad (7)$$

$$\eta=(E_{\mathrm{NPO}}/E_{\mathrm{AC}})^2\ , \quad (8)$$

$r=m_1/m_2$ is the ratio of heavy- and light-hole masses, ρ is the density of the material, $\bar{u}$ is the average sound velocity, and m_1^* is the effective mass of the charged carriers. We find acoustic and nonpolar optical deformation potentials of 4.5 and 7.5 eV, respectively. These results are in good quantitative agreement with other estimates[29] (3.5 and 6.5 eV, respectively), and our least-squares fit to the data (solid line) is in excellent agreement with the totality of our data. Further, these results show that, at high temperatures ($T\gtrsim70$ K), hole mobilities increase as $\mu\sim T^{-2.4}$—quantitatively identical to Hill's results[34] for majority-hole mobilities in high-purity p-type material obtained electrically, and also shown in Fig. 11. Here, again, we find minority-carrier mobilities *virtually identical* to those of majority-carrier mobilities, and our results and analysis are consistent with phonon-scattering limited transport.

Figure 12 shows the temperature dependence of both minority-hole and minority-electron mobilities, obtained as above, for our 0.30-μm heterostructure. In thin samples, such as this, where the influences of p-type modulation doping become significant—if not dominant ($\lesssim0.3$ μm)—as demonstrated at room temperature, we obtain mobilities for both species of minority-carrier electron and hole. Below 70 K, all transport in these structures is totally minority-electron dominated, at these excitation levels. We find that the resulting temperature-dependent minority-hole mobilities are identical, both qualitatively and quantitatively, with our 9.82-μm sample results and reported hole mobilities in high-purity, p-type GaAs.[34] Indeed, the lower solid line in Fig. 12 was obtained exactly as for Fig. 11, using Eq. (5).

Electron mobilities in GaAs are more complex than hole mobilities, with the dominant scattering mechanisms being polar-optical, acoustic-deformation-potential phonon (i.e., intrinsic), and piezoelectric scattering.[3] The dashed line in the figure represents the best, least-squares fit to our data using all three of these scattering mechanisms (and Mattheison's rule), together with each of these mechanisms individually indicated (solid lines).[3] Such fitting yields an acoustic-phonon deformation potential of 15.2 eV—with this as the only adjustable fitting parameter. Corresponding reported acoustic-phonon deformation potentials range from 7.0 to 18.0 eV.[3–6,35–37] Our result is, therefore, slightly higher than the most widely accepted value (13.5 eV),[5] and may be a result of differences in measurement technique and/or minority-

carrier versus majority-carrier mobilities.

In totality, our results indicate that minority-carrier transport is quantitatively identical to majority-carrier transport in these high-quality samples. Theoretically, minority-carrier mobilities may be expected to be smaller than majority-carrier mobilities, since impurity scattering may be more dominant for minority carriers (minority carriers have a lower Fermi energy than the same species as majority carrier, for the same doping levels).[25] However, we find that our minority-carrier mobilities, at these temperatures, are lattice limited, and are therefore truly intrinsic (phonon scattering), thus yielding minority-carrier mobilities comparable or even equal to corresponding majority-carrier mobilities.

V. CONCLUSIONS

We have used an all-optical PL-imaging technique to directly measure the transport of minority-carrier electrons and holes. Significantly, we find *all transport to be diffusive at all temperatures.* Also, both minority-electron and minority-hole mobilities obtained from our measured diffusion constants are in excellent quantitative agreement with electrical measurements of majority-electron and majority-hole mobilities. Additionally, our resulting temperature-dependent mobilities yield appropriate deformation potentials—indeed, ones in good agreement with majority-carrier, electrically determined values. Lastly, these results prove that our all-photoluminescence-based[24,26,27] carrier-transport-measurement technique is (1) fully analogous (but contactless) to the seminal, early optical Haynes-Shockly measurement[20] of transport, and (2) yields both qualitative and quantitative agreement with traditional all-electrical transport methods,[21–23] thus confirming its utility and accuracy.[38–40] Further, as will be discussed in future publications, this method performs equally well for both qualitative and quantitative measurement of neutral-particle (e.g., free excitons and plasmas) transport—an invaluable and complementary result which electrical-transport methods are entirely incapable of determining. Hence, for example, we may now study in detail, at all temperatures (e.g., 1.6–300 K), the spatial and temporal transport of both free carriers and free excitons, and, especially, their possible temperature-dependent joint (or coupled) transport properties.

ACKNOWLEDGMENTS

We thank L. M. Smith, G. A. Northrop, and J. Martinsen for useful discussions and assistance in computer-aided data acquisition. The IBM work was supported, in part, by the Office of Naval Research, under Contracts Nos. N00014-85-C-0868, N00014-90-C-0077, and N00014-91-J-1697. The work at Sandia was supported by the U.S. Department of Energy under Contract No. DE-AC04-76DP00789.

*Present address: Department of Chemical Engineering, University of Wisconsin, 1415 Johnson Drive, Madison, WI 53706.

[1]M. I. Nathan, W. P. Dumke, K. Wrenner, S. Tiwari, S. L. Wright, and K. A. Jenkins, Appl. Phys. Lett. **52**, 654 (1988).
[2]C. Guillemot, M. Baudet, M. Gauneau, A. Regreny, and J. A. Portral, Phys. Rev. B **35**, 2799 (1987).
[3]C. M. Wolfe, G. E. Stillman, and W. T. Lindley, J. Appl. Phys. **41**, 3088 (1970).
[4]B. Vinter, Phys. Rev. B **33**, 5904 (1986).
[5]P. J. Price, Phys. Rev. B **32**, 2643 (1985).
[6]P. J. Price, Surf. Sci. **143**, 145 (1984).
[7]J. P. Harrang, R. J. Higgins, R. K. Goodall, P. R. Jay, M. Laviron, and P. Delescluse, Phys. Rev. B **32**, 8126 (1985).
[8]C. T. Foxon, J. J. Harris, D. Hilton, J. Hewett, and C. Roberts, Semicond. Sci. Technol. **4**, 582 (1982).
[9]H. Sakaki, T. Noda, K. Hirakawa, M. Tanaka, and T. Matsusue, Appl. Phys. Lett. **51**, 1934 (1987).
[10]R. Gottinger, A. Gold, G. Abstreiter, G. Weimann, and W. Schlapp, Europhys. Lett. **6**, 183 (1988).
[11]R. Dingle, H. L. Störmer, A. C. Gossard, and W. Wiegmann, Appl. Phys. Lett. **33**, 665 (1978).
[12]H. Shtrikman, M. Heiblum, K. Seo, D. E. Galbi, and L. Osterling, J. Vac. Sci. Technol. B **6**, 670 (1988).
[13]B. J. F. Lin, D. C. Tsui, M. A. Paalanen, and A. C. Gossard, Appl. Phys. Lett. **45**, 695 (1984).
[14]J. H. English, A. C. Gossard, H. L. Störmer, and K. W. Baldwin, Appl. Phys. Lett. **50**, 1826 (1987).
[15]E. E. Mendez and W. I. Wang, Appl. Phys. Lett. **46**, 1159 (1985).
[16]R. Dingle, H. L. Störmer, A. C. Gossard, and W. Wiegmann, Appl. Phys. Lett. **55**, 1888 (1989).
[17]E. E. Mendez, P. J. Price, and M. Heiblum, Appl. Phys. Lett. **45**, 295 (1984).
[18]A. C. Gossard, J. H. English, M. Miller, and R. J. Simes, J. Cryst. Growth **95**, 247 (1989).
[19]W. I. Wang, E. E. Mendez, Y. Iye, B. Lee, M. H. Kim, and G. E. Stillman, J. Appl. Phys. **60**, 1834 (1986).
[20]J. R. Haynes and W. Shockley, Phys. Rev. **81**, 835 (1951).
[21]A. Olsson, D. J. Erskine, Z. Y. Xu, A. Schremer, and C. L. Tang, Appl. Phys. Lett. **41**, 659 (1982).
[22]H. Hilmer, A. Forchel, S. Hansmann, M. Morohashi, E. Lopez, H. P. Meier, and K. Ploog, Phys. Rev. B **39**, 10 901 (1989).
[23]R. K. Ahrenkiel, D. J. Dunlavy, D. Greenberg, J. Schlupmann, H. C. Hamaker, and H. F. MacMillan, Appl. Phys. Lett. **50**, 1329 (1987).
[24]G. D. Gilliland, D. J. Wolford, T. F. Kuech, and J. A. Bradley, Appl. Phys. Lett. **59**, 216 (1991); L. M. Smith, D. J. Wolford, J. Martinsen, R. Venkatasubramanian, and S. K. Ghandi, J. Vac. Sci. Technol. B **8**, 787 (1990).
[25]E. O. Kane, Solid State Electron. **28**, 3 (1985).
[26]G. D. Gilliland, D. J. Wolford, T. F. Kuech, J. A. Bradley, C. F. Tsang, and J. Martinsen (unpublished).
[27]D. J. Wolford, G. D. Gilliland, T. F. Kuech, L. M. Smith, J. Martinsen, J. A. Bradley, C. F. Tsang, R. Venkatasubramanian, S. K. Ghandi, and H. P. Hjalmarson, J. Vac. Sci. Technol. B **9**, 2369 (1991).

[28]We have assumed n_0 is constant, equal to the thick structure value, however allowing n_0 to vary—decreases as p_0 increases—($p_0 n_0$=const) will not quantitatively alter our results.

[29]J. D. Wiley, in *Semiconductors and Semimetals,* edited by R. K. Willardson and A. C. Beer (Academic, New York, 1975), Vol. 10.

[30]R. J. Nelson, in *Gallium Arsenide and Related Compounds,* IOP Conf. Proc. No. 45 (Institute of Physics, Bristol, 1979), p. 256.

[31]L. Jastrzebski, J. Lagowski, H. C. Gatos, and W. Walukiewicz, in *Gallium Arsenide and Related Compounds* (Ref. 30), p. 437.

[32]J. D. Wiley and M. DiDomenico, Jr., Phys. Rev. B **2**, 427 (1970).

[33]J. D. Wiley, Phys. Rev. B **4**, 2485 (1971).

[34]D. E. Hill, J. Appl. Phys. **41**, 1815 (1970).

[35]H. J. Lee, J. Basinski, L. Y. Juravel, and J. C. Woolley, Can. J. Phys. **47**, 233 (1979).

[36]J. A. Vergés, D. Glötzel, M. Cardona, and O. K. Andersen, Phys. Status Solidi B **113**, 519 (1982).

[37]S. J. Manion, M. Artaki, M. A. Emanuel, J. J. Coleman, and K. Hess, Phys. Rev. B **35**, 9203 (1987).

[38]G. D. Gilliland, D. J. Wolford, G. A. Northrop, T. F. Kuech, and J. A. Bradley, in *Gallium Arsenide and Related Compounds,* IOP Conf. Proc. No. 120 (Institute of Physics, Bristol, 1992), p. 413.

[39]D. J. Wolford, G. D. Gilliland, T. F. Kuech, J. A. Bradley, and H. P. Hjalmarson, in *Gallium Arsenide and Related Compounds* (Ref. 38), p. 271.

[40]G. D. Gilliland, D. J. Wolford, G. A. Northrop, M. S. Petrovic, T. F. Kuech, and J. A. Bradley, J. Vac. Sci. Technol. B **10**, 1959 (1992).